European Journal of Pharmaceutical Sciences 168 (2022) 106048

Contents lists available at ScienceDirect

European Journal of Pharmaceutical Sciences

journal homepage: www.elsevier.com/locate/ejps

Combination of lipid nanoparticles and iontophoresis for enhanced lopinavir skin permeation: Impact of electric current on lipid dynamics

Rayssa Barbary Pedroza Moura, Ms. [a], Lígia Marquez Andrade, Ph.D. [a], Lais Alonso, Ph.D. [b], Antonio Alonso, Ph.D. [b], Ricardo Neves Marreto, Ph.D. [a], Stephânia Fleury Taveira, Ph.D. [a,*]

[a] *Laboratory of Nanosystems and Drug Delivery Devices (NanoSYS), School of Pharmacy, Universidade Federal de Goiás (UFG), Rua 240, Setor Leste Universitário, Goiânia, GO 74605-170, Brazil*

[b] *Instituto de Física, Universidade Federal de Goiás (UFG). Av. Esperança, s/n, Campus Samambaia, Goiânia, GO 74690-900, Brazil*

ARTICLE INFO

Keywords:
Nanostructured lipid carrier
Lopinavir
Transdermal administration
Iontophoresis
Antiviral therapy
Electronic paramagnetic resonance

ABSTRACT

Nanostructured lipid carriers (NLC)-loaded with lopinavir (LPV) were developed for its iontophoretic transdermal delivery. Electronic paramagnetic resonance (EPR) spectroscopy of fatty acid spin labels and differential scanning calorimetry (DSC) were applied to investigate the lipid dynamic behavior of NLC before and after the electrical current. *In vitro* release and permeation studies, with and without anodic and cathodic iontophoresis were also performed. NLC-LPV had nanometric size (179.0 ± 2.5 nm), high drug load (~x223C 4.14%) and entrapment efficiency (EE) (~x223C 80%). NLC-LPV was chemically and physically stable after applying an electric current. The electrical current reduced EE after 3 h (67.21 ± 2.64%), resulting in faster LPV *in vitro* release. EPR demonstrated that iontophoresis decreased NLC lipid dynamics, which is a long-lasting effect. DSC studies demonstrated that electrical current could trigger the polymorphic transition of NLC and drug solubilization in the lipid matrix. NLC-LPV, combined with iontophoresis, allowed drug quantification in the receptor medium, unlike unloaded drugs. Cathodic iontophoresis enabled the quantification of about 7.9 μg/cm^2 of LPV in the receptor medium. Passive NLC-LPV studies had to be done for an additional 42 h to achieve similar concentrations. Besides, anodic iontophoresis increased by 1.8-fold the amount of LPV in the receptor medium, demonstrating a promising antiviral therapy strategy.

1. Introduction

Lopinavir (LPV) (Fig. 1) is an antiretroviral drug of great importance to control infection by the Human Immunodeficiency Virus (HIV), as it is a potent inhibitor of viral protease and has a high genetic barrier to mutations (Diaz, 2016). Recently, LPV has been used for patients with SARS-CoV-2 infection (COVID-19) (Liu et al., 2020). The use of LPV appears effective against COVID-19, but digestive adverse effects and hypokalemia prevented some patients from continuing with this treatment (Liu et al., 2020). The same adverse effects were also observed in HIV patients, such as diarrhea, nausea, vomiting, colitis (AbbVie, 2020). Probable adverse effects are related to its exclusive oral administration, which has low bioavailability.

LPV has low aqueous solubility (Fig. 1), making absorption difficult and variable (Kim et al., 2017; Maniyar and Kokare, 2019, Ravi et al. 2015). Besides, LPV is extensively compromised by the hepatic and intestinal first-pass metabolism, through the CYP4503A4 enzyme complex and by the P-glycoprotein, which, as well as the low aqueous solubility, contribute to reducing its oral bioavailability dramatically. To overcome this problem, LPV is co-administered with ritonavir, another protease inhibitor that acts by inhibiting CYP4503A4 and P-glycoprotein, increasing LPV bioavailability. However, high doses and a complex therapeutic regimen are necessary to make oral therapy effective (Pham et al., 2016; Patel et al., 2015).

Within this context, LPV transdermal administration could be a new strategy for both, administration to patients with HIV or for possible treatments of COVID-19, considering that transdermal delivery could reduce or eliminate different undesirable adverse effects. Transdermal delivery could also reduce the administered dose, simplify therapy, reduce toxicity, and positively impact patient adherence to the treatment (Ghosn et al., 2018; Puri et al., 2017; Iannazzo et al., 2015). Due to skin barrier function, LPV transdermal delivery has been limited due to its high molecular weight and lipophilicity (Maniyar and Kokare, 2019).

Several strategies have been studied to enhance LPV transdermal

* Corresponding author.
E-mail address: stephaniafleury@ufg.br (S.F. Taveira).

https://doi.org/10.1016/j.ejps.2021.106048
Received 6 May 2021; Received in revised form 19 October 2021; Accepted 20 October 2021
Available online 23 October 2021
0928-0987/© 2021 The Authors. Published by Elsevier B.V. This is an open access article under the CC BY license (http://creativecommons.org/licenses/by/4.0/).

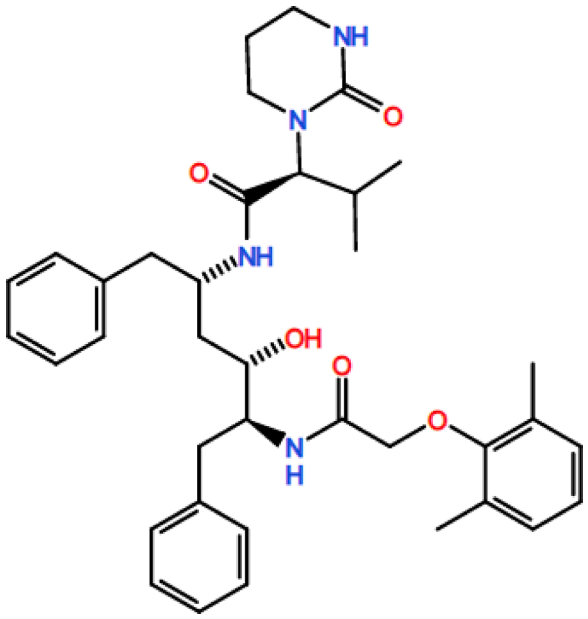

Fig. 1. Chemical structure of Lopinavir (LPV), molar mass of 628.8 Da, pKa of 13.39 and −1.5, Log P 4.69, and water solubility < 0.002 mg/mL.

delivery (Kim et al., 2017; Montenegro et al., 2016; Patel et al., 2015; Wang et al., 2018). For instance, Patel et al. (2015) combined physical (microneedles) and chemical methods to enhance LPV transdermal delivery. The combined therapy resulted in higher permeation of the drug, and bioavailability greater than oral suspension (Patel et al., 2015). Kim et al. (2017) solely used physical method (reverse electrodialysis) and obtained LPV permeation at low doses (ng/cm^2). Nanosystems have also been proposed, such as niosomes, ethosomes (Patel et al., 2012), and solid lipid nanoparticles (SLN) (Ansari et al., 2018). In general, nanosystems improved drug permeation in more than 24 h of study.

The combination of passive and active strategies has become more frequent to enable transdermal delivery in a shorter period, which is quite advantageous for antiviral therapy. Among various delivery systems, iontophoresis has demonstrated exceptional interest as a helpful tool for enhancing skin permeation of large-sized molecules (Kalia et al., 2003; Krishnan et al., 2014). Although iontophoresis has proven significant benefits, LPV iontophoretic delivery has not been investigated yet. Besides, the combination of lipid nanoparticles and iontophoresis has been unexplored in the literature (Taveira et al., 2014; Charoenputtakun et al., 2015; Huber et al., 2015). Therefore, a detailed investigation of the effects of electrical current in LPV-loaded nanostructured lipid carriers (NLC) can bring relevant information about the feasibility of LPV transdermal delivery.

It is worth noticing that NLC are lipid nanocarriers comprised of a mixture of solid and liquid lipids, with a lipid matrix solid at room and body temperature (Shah et al., 2011; Fang et al., 2013). Surfactants are used to stabilize the lipid matrix, and NLC were developed to enhance drug loading and stability (Fang et al., 2013; Charoenputtakun et al., 2015). Moreover, iontophoresis is a non-invasive technique that applies a low-density electrical current (0.5 mA/cm^2) to deliver charged and uncharged molecules to deeper skin layers (Taveira et al., 2014; Petrilli and Lopez, 2018). Thus, we hypothesized that cathodic iontophoresis could push negatively charged lipids from NLC into stratum corneum (SC), favoring LPV close contact with the skin and its partition to deeper layers. Alternatively, anodic iontophoresis could favor LPV electroosmotic delivery after drug release from NLC. In both cases, NLC could contribute to drug permeation due to its interaction with SC, causing lipid rearrangements and, consequently, enhancing drug diffusion (Garcês et al., 2018; Fang et al., 2013). Still, little is known about the influence of electrical current on lipid nanoparticles' matrices. Our research group has already demonstrated that the drug release can be accelerated by iontophoresis (Taveira et al., 2014). However, it is still necessary to investigate the effect of the electrical current on the lipid dynamics of NLC.

To test these hypotheses, LPV-loaded NLC was produced based on drug solubility in different surfactants. NLC-LPV was fully characterized, and stability was studied. Electronic paramagnetic resonance (EPR) spectroscopy of a spin-labeled stearic acid was used as a complementary technique to investigate the lipid dynamic behavior of NLC before and after the electrical current. Also, it was evaluated whether the effect of electrical current was long-lasting to NLC lipidic matrices. *In vitro* release and permeation studies, with and without anodic and cathodic iontophoresis, were also performed.

2. Materials and methods

2.1. Reagents

LPV (≥ 99%) (MW 628.8 Da) was kindly donated by Cristália Indústria Farmacêutica (Itapira, Brazil) and IQUEGO (Indústria Química do Estado de Goiás, Goiânia, Brazil). HPLC grade acetonitrile was purchased from J. T. Baker (Phillipsburg, NJ, USA). Tween® 80, Span® 80, Span® 85, Pluronic® F-127, Pluronic® F-68, sodium taurodeoxycholate, oleic acid and spin label (5-doxyl stearic acid, 5-DSA) were purchased from Sigma Aldrich (St. Louis, MO, USA). Plurol® Oleic CC, Gelucire® 48/16 and Labrasol® were kindly donated by Gattefossé (France). Stearic acid (mp 58.77 °C) was from Vetec (São Paulo, Brazil). Ultrapurified water was used. All other chemicals were of analytical grade.

2.2. Analytical procedure

LPV was assayed using a UV high-performance liquid chromatography method (HPLC) validated following ICH (2005) guidelines. The HPLC system consisted of a quaternary pump (G7111B), autosampler (G7129A), and UV detector (G7114A) (Agilent 1260 Infinity II, Agilent Technologies®, USA). The separation was achieved using an Agilent ZORBAX® Eclipse Plus C18 column (250 × 4.6 mm, 5 μm). The mobile phase was a 70:30 (v/v) mixture of acetonitrile and water. The flow rate was 1.0 mL/min, the injection volume was 20 μL and UV detection was 210 nm. Data acquisition was performed using Openlab® software (Agilent technologies®, USA).

LPV retention time was 4.6 min. A linear calibration curve was obtained ($y = 970584x - 35{,}161$; $r = 0.9999$) and the test-F ($F = 1.04$) was calculated based on the analysis of different concentrations (0.5–10 μg/mL). The limit of quantitation (LOQ) of the method was 0.5 μg/mL. Selectivity was investigated (formulation components and skin homogenate), and no interference was observed in drug retention time.

2.3. Solubility study

LPV solubility was evaluated in different surfactants (lipophilic and hydrophilic) for NLC production. For lipophilic surfactants (Plurol® Oleic CC - HLB 3.0, Span® 80 - HLB 4.3 e Span® 85 - HLB 1.8), an excess of the drug (approximately 65 mg/mL) was added in 1 mL of each surfactant. 1% (w/v) of hydrophilic surfactants (Tween® 20 - HLB 16.7, Gelucire® 48/16 - HLB 12, sodium taurodeoxycholate - HLB 23, Tween® 80 - HLB 15, Pluronic® F-68 - HLB 29, Pluronic® F-127 - HLB 18 to 23, Labrasol® - HLB 12) were dispersed in purified water ($n = 3$). LPV was added in excess (approximately 10 mg/mL). All samples were kept under magnetic stirring at 300 rpm for 24 h, at 25 ± 2 °C. At the end, they were filtered, diluted in acetonitrile, and injected into HPLC system to determine the LPV content.

2.4. Production of nanostructured lipid carriers (NLC) containing lopinavir (LPV) (NLC-LPV)

Lopinavir-loaded NLC (NLC-LPV) was prepared using the microemulsion technique (Andrade et al., 2017). A mixture of Tween® 80, Span® 85, stearic acid, and oleic acid was heated, and LPV was added to the melted material. After that, 250 μL of distilled water was added to the mixture under magnetic stirring, and a microemulsion was obtained. The microemulsion was dispersed into cold distilled water (2–4 °C) at 13,400 rpm for 10 min with T18 basic ULTRA-TURRAX® (IKA, Staufen, Germany). A microemulsion:water ratio of 1:20 was applied to obtain NLC dispersion. NaCl (201 mM) was added in all NLC formulations to ensure the electrical current passage during iontophoresis experiments.

The dispersion had a total lipid content of 2% (w/v) (stearic acid at 15 mg/mL and oleic acid at 5 mg/mL) and, stabilized by 1.25% (w/v) of surfactant (Tween® 80 at 2 mg/mL and Span®85 at 10,5 mg/mL). The final volume of the dispersion was 20 mL (Andrade et al., 2017). Different concentrations of LPV were added (0.5 to 1.5 mg/mL). Nanoparticles without LPV were also obtained (NLC) and used as controls.

2.5. Characterization of lipid nanoparticles (NLC and NLC-LPV)

Mean diameter, PdI, and zeta potential of NLC and NLC-LPV (1.5 mg/mL) were determined in triplicate using a Zetasizer ZS (Malvern Instruments, UK). The entrapment efficiency (EE) of LPV was determined by centrifugation Silva et al., 2016). Briefly, 1 mL of freshly prepared nanoparticle dispersion was subjected to centrifugation (EXCELSA® 205/208 centrifuge, FANEM®, São Paulo, Brazil) for 20 min at 4200 rpm and 25 °C, to separate unloaded drug (precipitate) and loaded drug (supernatant). An aliquot of the supernatant was solubilized with acetonitrile and withdrawn for HPLC analysis. LPV content in NLC was determined by lipid disruption with acetonitrile, followed by HPLC quantification. All analyses were performed in triplicate. Entrapment efficiency (EE), drug loading (DL), and drug recovery (DR.....) were calculated according to Eqs. (1) to ((3), respectively.

$$EE\ (\%,\ w/w) = \frac{amount\ of\ encapsulated\ LPV}{amount\ of\ LPV\ in\ the\ formulation}\ x\ 100 \quad (1)$$

$$DL\ (\%,\ w/w) = \frac{amount\ of\ encapsulated\ LPV}{weight\ of\ the\ lipids}\ x\ 100 \quad (2)$$

$$DR\ (\%,\ w/w) = \frac{amount\ of\ LPV\ in\ the\ formulation}{theoretical\ amount\ of\ LPV}\ x\ 100 \quad (3)$$

2.6. Morphological characterization

The average diameter and nanoparticle morphology were also studied by transmission electron microscopy (TEM) (JEOL, JEM-2100, Tokyo, Japan) equipped with an energy dispersive spectrometry (EDS) (Thermo Scientific®, Tokyo, Japan). The images were captured with a GATAN BioScan camera, Model ORIUS SC 200 CCD (Gatan, CA, USA) using the Digital Micrograph 3.6.5 software (Gatan, CA, USA). One drop of the diluted sample (20-fold) was deposited on the copper grid (300 mesh; Electron Microscopy Sciences, PA). After drying, the excess sample was removed, and a drop of uranyl acetate (2%) was placed on the grid, air-dried, and analyzed under a tension of 200 kV.

2.7. Short-term stability studies

Stability studies were performed with the NLC-LPV (1.5 mg/mL). The nanoparticles dispersion was analyzed immediately after preparation and then stored at 25 ± 2 °C for 25 days. Stability was evaluated by comparing the initial mean diameter, PdI, EE, and DR with those obtained from samples after 8, 14, and 25 days of storage.

2.8. Stability in the presence of electrical current

2.8.1. LPV dispersion

LPV electrical stability was performed by applying an electric current of 0.5 mA/cm^2 for 6 h using Ag/AgCl electrodes. An external power supply – ActivaDose II (Activa Tek, Salt Lake City, USA) was used. Formulation consisted of a drug dispersion in the water at 1.0 mg/mL and 201 mM NaCl. Samples were collected at 6 h of the current application, and the LPV content determined according to Section 2.2. Analyzes were performed in triplicate.

2.8.2. NLC-LPV

NLC-LPV (1.5 mg/mL) were produced with 201 mM NaCl and subjected to electric current (0.5 mA/cm^2) for 6 h. Samples were collected at 0.5, 3, and 6 h and evaluated for EE and DR. Mean diameter, PdI, and zeta potential were also evaluated at the end of the experiment (6 h). The analysis was performed in triplicate.

2.8.3. EPR spectroscopy measurements with and without electrical current

NLC-LPV (1.5 mg/mL) were spin-labeled, according to Andrade et al. (2017). Briefly, NLC dispersions were incubated, at room temperature, with an aliquot (0.5 μL) of a stock solution of 5-DSA (5 mg/mL). The samples were gently agitated and placed in a capillary tube, which was flame sealed for the EPR measurements.

Samples were analyzed before and immediately after the application of 0.5, 1, 2, and 3 h of electric current at 0.5 mA/cm^2. Samples subjected to electric current (1, 2, and 3 h) were kept at rest for 1 h, and 24 h and EPR measurements were also performed.

The measurements were conducted at 25 ± 1 °C using an EMX-Plus spectrometer (Bruker®, Rheinstetten, Germany). The instrument parameters were as follows: microwave power, 20 mW; modulation frequency, 100 kHz; modulation amplitude, 1.0 G; magnetic field scan, 100 G; sweep time, 168 s; and detector time constant, 41 ms. As in previous studies (Andrade et al., 2017; Tosta et al., 2014), the dynamics of the medium was evaluated by the spectral parameter $2A_{//}$ for the marker 5-DSA. The lower the value of $2A_{//}$, the higher the mobility of the medium.

2.9. Differential scanning calorimetry (DSC) studies

DSC analysis was performed using a Netzsch® DSC 204 F1 Nevio (Selb, Germany). First, NLC and NLC-LPV dispersions were submitted to electrical current (0.5 mA/cm^2) for 3 h. Then, to obtain powder samples, NLC dispersions were first concentrated using an ultrafiltration system (Vivaspin 2® Sartorius, Bohemia, USA), centrifugated at 4000 rpm. The samples were then frozen at −80 °C for 12 h and lyophilized using a freeze-drying system at a pressure of 2.0 Pa (Thermo Fischer Scientific, Waltham, USA). The dried samples were put into standard aluminum crucibles (about 4 mg), and DSC curves were obtained under a dynamic nitrogen atmosphere (50 mL/min) at a heating rate of 10 °C/min over a temperature range from 30 to 100 °C. NLC without the application of electrical current was also lyophilized and analyzed. Pure LPV and stearic acid were evaluated and were used for comparison.

2.10. Drug release

In vitro drug release was assessed using a Franz-type diffusion cell (Unividros®, São Paulo, Brazil). A cellulose acetate membrane (MWCO 12,000–14,000, Fisher Scientific®, UK) was used between the donor and the receiver chamber. The receptor compartment was filled with 15 mL of HEPES buffer (25 mM) with 5% Tween® 80 and 201 mM NaCl (pH = 5.3), maintained at 37 °C and 300 rpm of stirring rate. Donor compartment was filled with 1.7 mL of NLC-LPV dispersion in water (1.5 mg/mL) (pH ~x223C 5.0) and LPV dispersion in HEPES buffer (unloaded drug at 1.5 mg/mL) (pH ~x223C 5.0) as a control. Cathodic and anodic iontophoretic drug release was performed by placing a

negative and positive electrode in the donor compartment, respectively. An 0.5 mA/cm^2 electrical current was provided by an external power supply (ActivaDose II, Activa Tek, Salt Lake City, USA). These studies were compared to passive studies (without electrical current) at the same conditions. After 6 h, 1 mL of the receiver solution was withdrawn ($n \geq 6$). The released amount of LPV was determined by HPLC, according to Section 2.2.

2.11. In vitro permeation studies

Passive and iontophoretic permeation (cathodic and anodic) were performed with the same vertical flow-through diffusion and experimental conditions as release studies (Section 2.10). Epidermis (EP) from porcine ear skin was separated from the remaining skin by hot technique, according to Silva et al. (2016) and placed between donor and receptor chamber. The formulations were applied to the skin surface, as described for the synthetic membrane, and the LPV was 1.5 mg/mL. The available diffusion area was 1.87 cm^2. After 6 h studies, the EP was removed from diffusion cells, cut into small pieces, and immersed in 5 mL of acetonitrile. Then, samples were submitted to bath sonication (20 min) (USC 1400, Unique, Indaiatuba, Brasil) and vortex homogenization. Subsequently, samples were filtered and analyzed on HPLC (according to Section 2.2). The LPV recovery from EP was 101.11 ± 9.64%.

2.12. Statistical analysis

Data collected were processed using GraphPad Prism v.5.01 software (GraphPad Software, CA, USA). Each experiment's statistical significance was analyzed by one-way ANOVA, followed by Tukey's multiple comparisons. Tests yielding p values of < 0.05 were considered significant.

3. Results and discussion

3.1. LPV solubility

Drug solubility in melted lipids and surfactants may influence EE and DL (Souza et al., 2011; Teixeira et al., 2018). Thus, to reach the best efficiency of NLC, LPV solubility in different excipients was considered. For instance, LPV has high solubility in stearic acid (563 mg/mL) and oleic acid (400 mg/mL) (Garg et al., 2019; Patel et al., 2016), which were chosen to be NLC lipid matrix. LPV showed great solubilization in Span® 85 (lipophilic surfactant) and Gelucire® 48/16 (hydrophilic surfactant) (Table S1 – supplementary material). However, Gelucire® 48/16 prevented microemulsion formation, a prerequisite for NLC production by the selected technique, therefore, it was excluded from further studies. Tween® 80 provided a higher drug solubilization when compared to other hydrophilic surfactants ($p < 0.05$) (Table S1 – Supplementary Material) and was chosen together with Span® 85 for NLC production.

3.2. Production and characterization of NLC-LPV

Unloaded and NLC-LPV were produced by microemulsion technique with stearic acid, oleic acid, Tween® 80, and Span® 85 (Table 1). Monodisperse NLC formulations, with negative zeta potential, were successfully obtained. The increase of LPV content in lipid nanocarriers significantly enhanced DL ($p < 0.05$).

An increase in particle size with the increase of drug concentration was observed ($p < 0.05$) (Table 1), as already reported in the literature (Patel et al., 2019; Stella et al., 2018). Possibly, the excess of drug not associated with the lipid matrix may have been solubilized at the interface, causing an approximately 20 nm increase in the particle size. For nanoparticles in which the drug preferably associates at the surface, increases of 300–400 nm range have already been reported (Stella et al., 2018).

EE and DL obtained here were in good agreement with previous findings where high EE (~x223C 83%) and drug loading were obtained for compritol, oleic acid, and Tween 80® based-NLC loaded with LPV (Garg et al., 2019).

Zeta potential values indicate NLC high stability, considering that a zeta potential equal to or greater than |30| mV indicates less aggregation probability due to electrostatic repulsion (Andrade et al., 2017; Zhong and Zhang, 2019). The negative zeta potential values are probably the result of negative residual charges of stearic acid and oleic acid (Souza et al., 2011; Taveira et al., 2012). Zeta potential increased (in modulus) with the addition of 1.5 mg/mL of LPV even though LPV is a neutral molecule. At this concentration, LPV had probably reached the maximum drug loading, requiring surfactants molecules to solubilize the drug in the aqueous medium of the formulation. Thus, the increase in zeta potential magnitude is related to the surfactant migration from the NLC surface, which resulted in a lower surface coverage, exposing the negative charges of stearic acid.

DR. Raged from 69.17 ± 6.80 to 71.96 ± 9.54%, in agreement with other reports (Souza et al., 2011; Taveira et al., 2012; Tosta et al., 2014). Drug loss is associated with formulation loss in homogenizing equipment (Silva et al., 2012).

Formulations with 1.5 mg/mL of LPV seemed to be the most promising since most of the characteristics have been maintained, and greater DL may contribute to drug skin flow (Table 1). It is well described in the literature that drug diffusion into the skin is related to the drug concentration applied to the skin surface (Tosta et al., 2014).

3.2.1. Morphologic characterization of NLC-LPV

The morphological analysis (Fig. 2) by transmission electron microscopy (TEM) showed structures with a spherical shape and size of about 200 nm, corroborating with mean diameter obtained by dynamic light scattering technique. Besides, it is possible to observe lines or lamellae structures in NLC lipid matrix (Fig. 2C and D), which may indicate fatty acid chain union, possibly achieved with the crystallization process (Gordillo-Galeano and Mora-Huertas, 2018). In contrast, Fig. 2D demonstrates some regions in NLC matrix with the absence of these structures, suggesting the presence of liquid lipids, which may difficult the fatty acid organization. These findings reinforce the theory that liquid lipids increase lipid matrix disorganization, contributing to enhance drug load and to avoid or minimize drug expulsion during storage time. (Czajkowska-Kośnik et al., 2019). Therefore, it is believed that the liquid lipid is randomly distributed in the NLC matrices, including on the surface. These findings have also been suggested in the literature (Tosta et al., 2014; Andrade et al., 2017; Gordillo-Galeano and

Table 1
Mean diameter (nm), polydispersity index (PdI), zeta potential (mV), drug loading (DL), and entrapment efficiency (EE) of unloaded NLC and NLC-LPV with different concentrations of LPV. Values represented as mean ± standard deviation ($n \geq 3$). *$p < 0.05$.

	LPV(mg/mL)	Mean diameter (nm)	PdI	Zeta potential (mV)	DL (%, w/w)	EE (%, w/w)
NLC	–	139.40 ± 3.08	0.155 ± 0.008	−27.3 ± 0.7	–	–
NLC-LPV	0.5	145.83 ± 5.23	0.195 ± 0.002	−30.4 ± 0.7	2.48 ± 0.08	101.70 ± 4.88
	0.7	139.70 ± 7.21	0.178 ± 0.014	−28.8 ± 0.6	3.13 ± 0.11	83.80 ± 2.89*
	1.0	151.50 ± 7.24	0.196 ± 0.032	−30.8 ± 0.9	4.12 ± 0.40	82.38 ± 7.93*
	1.5	179.00 ± 2.55*	0.182 ± 0.035	−37.5 ± 0.8*	5.63 ± 0.12*	78.84 ± 4.87*

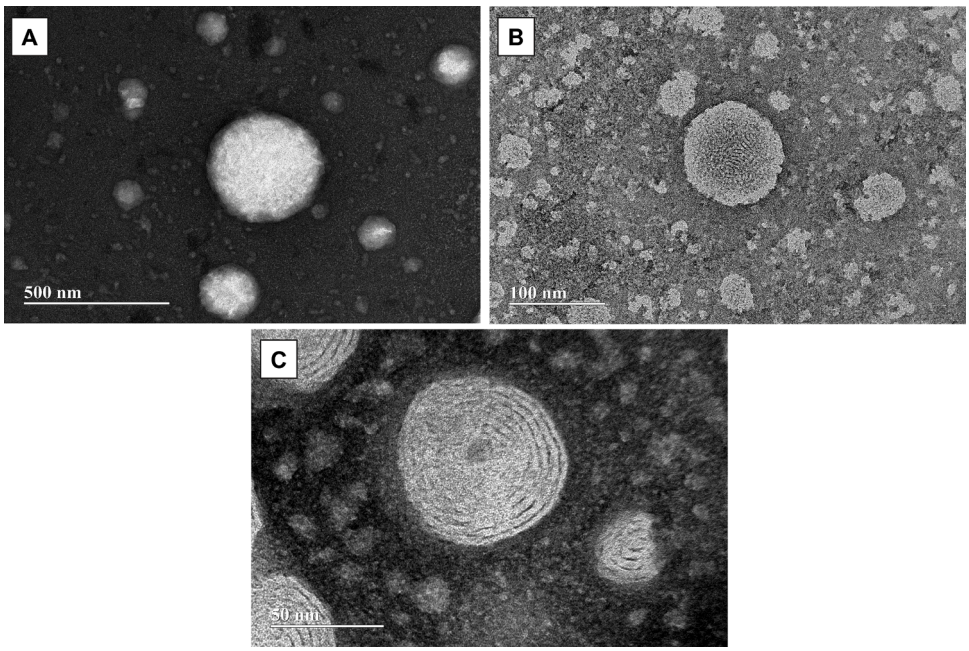

Fig. 2. Transmission Electron Microscopy (TEM) of NLC-LPV (1.5 mg/mL). The images were taken with magnifications of 15,000x (A), 50,000x (B), and 120,000x (C) and the scale bar measured in nm.

Mora-Huertas, 2018)

3.3. Stability studies

Stability studies were performed with NLC-LPV (1.5 mg/mL). Nanoparticles were stored at 25 ± 2 °C for 25 days, and the mean diameter, PdI, zeta potential, EE and DR were determined from both freshly prepared and aged samples (Table 2). NLC-LPV had high stability, as the mean diameter, PdI, EE and DL did not show any significant change ($p > 0.05$). In contrast, the zeta potential showed a significant change in the first 8 days of storage ($p < 0.05$), with no further variation until the end of the study. The reduction in the pH from 5.4 to 4.8 indicates the dissociation of stearic acid, an increase in the ionic strength of the medium, resulting in a zeta potential decrease (Shah et al., 2014; Gordillo-Galeano et al., 2021). Fortunately, these changes did not cause any aggregation of NLC-LPV formulations, probably due to additional steric stabilization promoted by surfactants (Mitri et al., 2011). EE was maintained during storage (Table 2), possibly due to drug affinity to NLC lipid matrix (Tosta et al., 2014).

3.4. Stability in the presence of electrical current

The analysis of the effect of the electric current in both unloaded and encapsulated drug (NLC-LPV) aimed to evaluate the chemical stability of the drug, as well as the influence of electric current on the NLC physical stability.

Table 2
Mean diameter (nm), polydispersity index (PdI), zeta potential (mV), entrapment efficiency (EE), and drug loading (DL) of freshly prepared NLC-LPV (1.5 mg/mL) and aged NLC-LPV after storage at 25 ± 2 °C for 25 days. Values represented as mean ± standard deviation ($n \geq 3$). Symbols indicate $p < 0.05$.

Time (day)	Mean diameter (nm)	PdI	Zeta potential (mV)	EE (%, w/w)	DL (%, w/w)
0	188.27 ± 4.39	0.211 ± 0.019	−42.1 ± 1.3*	75.10 ± 1.66	5.63 ± 0.12
8	185.60 ± 5.11	0.212 ± 0.012	−46.2 ± 6.2*	75.27 ± 1.42	5.65 ± 0.11
14	187.83 ± 2.94	0.162 ± 0.008	−32.3 ± 0.5	77.08 ± 0.95	5.78 ± 0.07
25	179.16 ± 6.10	0.204 ± 0.037	−32.8 ± 1.1	74.96 ± 3.31	5.62 ± 0.25

At the end of 6 h of study, the recovery of unloaded LPV was 92.40 ± 1.02%, and for NLC-LPV was 102.75 ± 7.27%. Drug recovery in NLC-LPV indicates no LPV chemical degradation due to electrical current application

Fig. 3 demonstrates NLC-LPV characterization without and with the application of electrical current for 6 h.

Mean diameter and PdI were remarkably similar after the current application, demonstrating excellent physical stability of NLC-LPV (Fig. 3a), even with the significant reduction of zeta potential (Fig. 3b). Probably the steric stabilization achieved with surfactants maintained the physical stability during electrical current application (Zimmermann and Müller, 2001).

It is interesting to note that, EE significantly decreased even with a shorter time of application of the electric current (3 h) (Fig. 3c), indicating that the electrical stimulus can act as a trigger for drug release from the lipid matrix. This finding is quite interesting for obtaining more sophisticated drug delivery systems, which can be triggered by an external physical stimulus. In this context, lipid particles are great systems for lipophilic drugs such as LPV, as they guarantee excellent stability, EE, and DL. However, drug release is hampered (see Section 3.6), due to high drug affinity to the lipid matrix and surfactants. Thus, the increase in drug expulsion with the electric current is fundamental to increase drug release and, consequently, the permeation of the drug to deeper skin layers. To better study the effects of electrical current in an NLC-LPV lipid matrix, EPR spectroscopy and DSC studies were performed.

3.5. EPR spectroscopy

The EPR study was carried out to evaluate the influence of the electric current (0.5 mA/cm^2) on the lipid dynamics of the NLC-LPV matrix. Therefore, EPR was measured before and after the application of the electrical potential (Fig. 4).

The EPR spectrum of spin label 5-DSA incorporated into the NLC is commonly characterized by a broad line-shape with the resolution of the outer hyperfine splitting, denoted as $2A_{//}$, which is a parameter directly

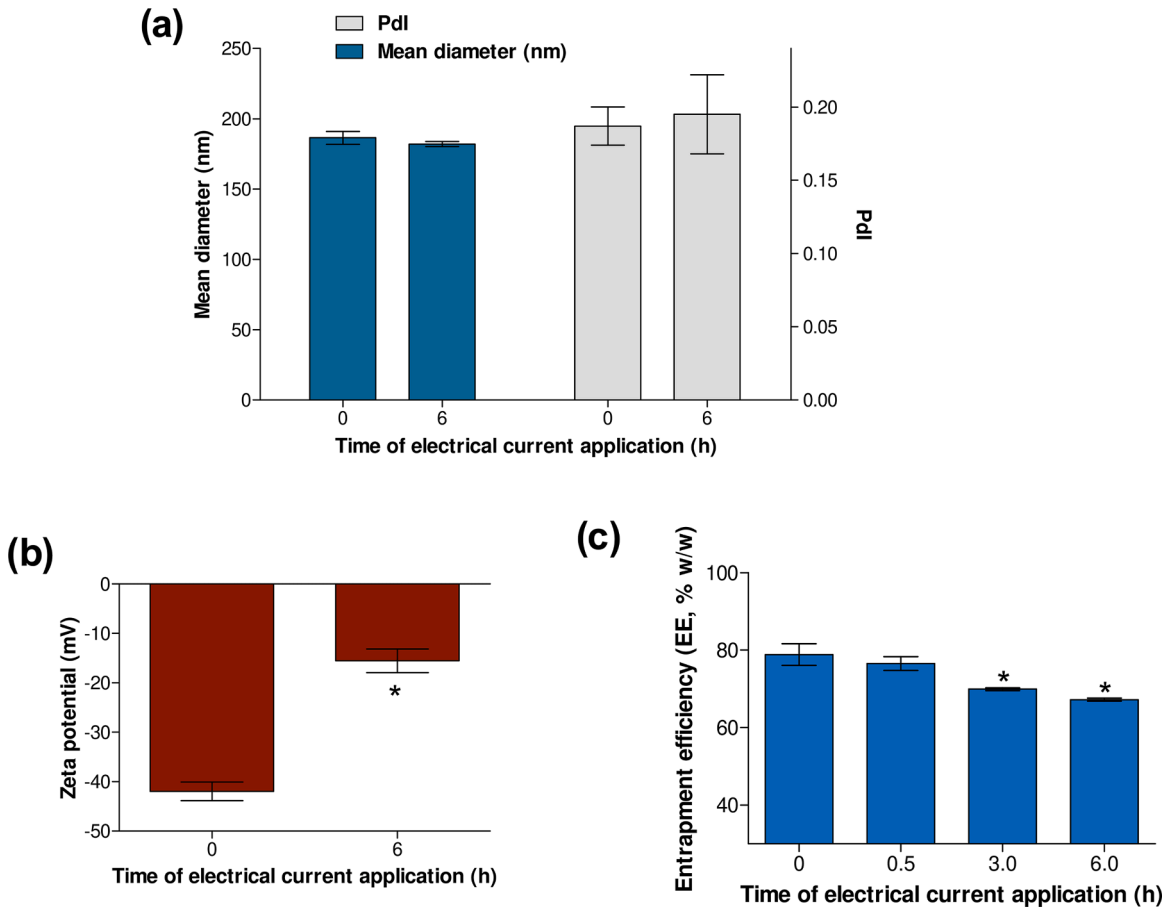

Fig. 3. Characterization of NLC-LPV (1.5 mg/mL) with or without application of electrical current (0.5 mA/cm2) for a maximum of 6 h ($n \geq 3$): (a) Mean diameter (nm) and polydispersity index (PdI), (b) zeta potential (mV) and (c) entrapment efficiency (%, w/w). *$p < 0.05$.

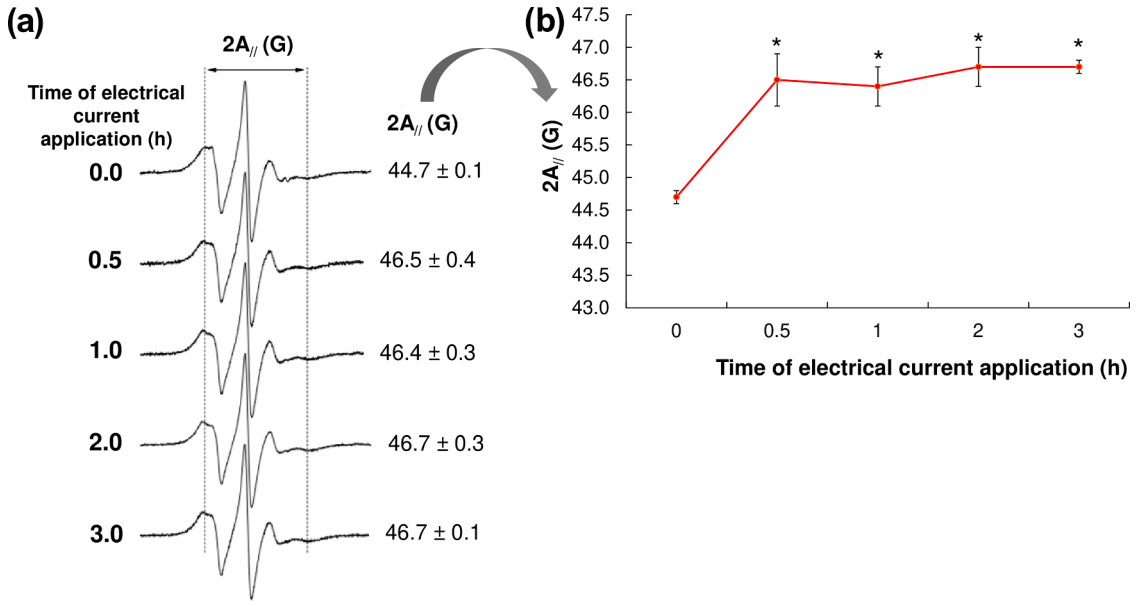

Fig. 4. EPR spectra and 2A// values for NLC-LPV (1.5 mg/mL), spin labeled with 5-DSA, without application of electric current and with application of electrical current (0.5 mA/cm2) for 0.5, 1, 2 and 3 h: (a) the EPR spectra and measurements of parameter 2A// and (b) 2A// plotted in relation to the time of application of the electric current. *$p < 0.05$.

measured in the EPR spectrum as shown in Fig. 4a (Andrade et al., 2017; Da Rocha et al., 2019; Tosta et al., 2014). $2A_{//}$ is an EPR parameter, which has been widely used to characterize the rotational rates of the spin-labeled lipid chain segments even though it is, in principle, a static parameter associated with the orientational distribution of the nitroxide radical moiety in the lipid bilayer (De Queirós et al., 2005).

Fig. 4 shows a significant increase in $2A_{//}$ values after the application of electric current ($p < 0.05$). The increase of approximately 2.0 G indicates the decrease of lipid dynamics when an electrical current is applied to NLC-LPV. Also, the increase in duration of the electrical current application did not linearly increase lipid rigidity, i.e., 30 min was enough to achieve greater values of $2A_{//}$.

Previous studies carried out by our research group have shown that solid lipid nanoparticles (SLN) are more rigid than NLC (ndrade et al., 2014; Tosta et al., 2014), due to higher lipid packing density of SLN. Thus, more organized lipid matrices have shown to be more rigid (Tosta et al., 2014). It is well described in the literature that lipid nanoparticles suffer lipid crystallization, going from a higher energy state to a more stable one. i.e., more disorganized to more organized lipid matrices, even for NLC (Gordillo-Galeano and Mora-Huertas, 2018). One of the hypotheses is that electrical current triggered the polymorphic modifications by increasing lipid packing density and increasing NLC rigidity after electrical current (Fig. 4). It has not been described in the literature that the electric current could accelerate the polymorphic transitions in colloidal systems. However, it is already known that some external factors can accelerate or minimize these transitions, such as temperature, drying processes (Gordillo-Galeano and Mora-Huertas, 2018; Santos et al., 2018), and others. For instance, Shah et al. (2011) reported lipid matrix modification when nanoparticle dispersions had contact with new surfaces, such as a syringe needle, increasing formulation viscosity. Although this hypothesis is feasible, it is not possible to prove through the EPR studies that electrical current trigged the polymorphic transition. What is known is that electric current changed the matrix fluidity, resulting in a rigid matrix with a reduction in EE (Section 3.4). It is known that drug expulsion from lipid matrices has been related to polymorphic lipid transitions (Jores et al., 2003) and, therefore, DSC studies were performed with formulations before and after applying an electric current (Section 3.5).

Another essential fact to be emphasized is that the change in lipid dynamics, was a long-lasting effect, i.e., the electric current increased the values of $2A_{//}$ and they remained similar after 1 and 24 h after electrical current application ($p > 0.05$) (Fig. S1 – Supplementary Material). These findings also corroborate the hypothesis of polymorphic change in lipid matrices (Gordillo-Galeano and Mora-Huertas, 2018). However, others phenomenon could also be related to the change in lipid fluidity. Fang et al. (1999) proposed that electrical fields stabilize lipid bilayers' pores, contributing to liposomes' physical stability. It was also reported that the electrical field could cause motion of electrolytes and lipids, having a similar effect as sonication, i.e., giant liposomes under sonication could reduce vesicle size and produce smaller liposomes. Although some papers mention the effects of iontophoresis in liposomes (Fang et al., 1999) and micellar systems (Chopra et al., 2012, 2013; Sarvaiya et al., 2013), little is known about these effects in lipid nanoparticles. It is possible that electrical current acts as the sonication technique, as Behbahani et al. (2017) described. They demonstrated that the increase in sonication time resulted in more interaction between aqueous e lipid phases, which decreased EE of lipid nanoparticles.

In summary, the electric current application led to a more rigid lipid matrixes, resulting in a faster drug release with the electrical stimulus (see Section 3.6). This fact reinforces the idea that this strategy can be exciting when it is desired to trigger the release of the drug, which may eventually favor its permeation into the skin.

3.6. DSC studies

DSC curves of NLC (unloaded) with and without the application of iontophoresis are presented in Fig. 5a. Also, pure stearic acid was analyzed. The DSC curve of pure stearic acid showed its melting peak at 59.6 °C (onset temperature at 51.7 °C and ends at 63.2 °C), probably due to the presence of polymorph B (Maretti et al., 2021). The broad shape suggests other polymorphs, as at least four polymorphic forms have been already identified (Teixeira et al., 2010). NLC (blue curve – Fig. 5a) did not present the characteristic melting peak of stearic acid. The production method and the addition of oleic acid resulted in the amorphization of the solid lipid, suppressing the stearic acid melting peak in NLC formulations (Maretti et al., 2021). However, three different melting peaks appear in the DSC curve of NLC after applying electrical current (T_{peak} of 62.7, 63.9, and 67.4 °C). These peaks may be related to the stearic acid crystallization in different polymorphic forms (Teixeira et al., 2010). Comparing and identifying these polymorphous is not always feasible due to the differences in the heating rate and mixtures with oleic acid (Sato 1987Sato, 1987). Thus, as hypnotized in EPR studies, the electrical current could trig the polymorphic transition in lipid matrices, resulting in significant changes in lipid dynamic fluidity.

Fig. 5b demonstrates NLC-LPV DSC curves before and after iontophoresis application. Also, pure LPV was analyzed for comparison. LPV curve shows its melting peak at 94.3 °C, which is following the literature (Negi et al., 2013). NLC-LPV (without applying electrical current) showed a similar broader peak at 93.4 °C, denoting LPV loading in molecular and crystalline states. Surprisingly, applying an electrical current suppressed the LPV peak in DSC curves of NLC-LPV (iontophoresis) (Fig. 5b). Also, stearic acid melting peaks observed in unloaded NLC after iontophoresis (Fig. 5a) were not observed in these samples (NLC-LPV iontophoresis) (Fig. 5b). It was demonstrated that the application of electrical current reduced the EE (Fig. 3), yet most of the drug was still present in the lipid matrix. Thus, the electrical current also favored LPV solubilization in the lipid matrix, resulting in the suppression of LPV peak in DSC curves of NLC-LPV (iontophoresis). Probably the LPV solubilization hampered the recrystallization of stearic acid observed in unloaded NLC submitted to iontophoresis. In summary, the

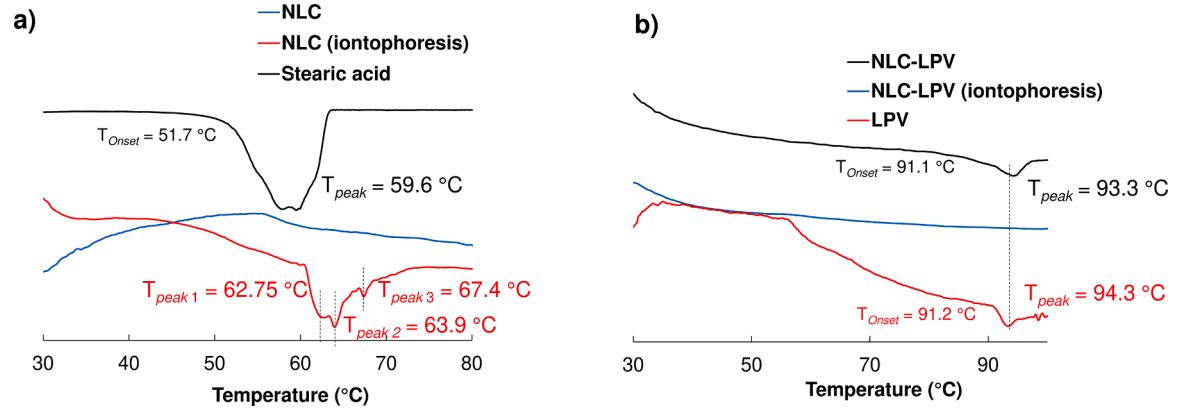

Fig. 5. DSC curves of (a) unloaded NLC (with and without application of iontophoresis) and pure stearic acid, (b) NLC-LPV (with and without application of iontophoresis) and pure LPV.

electrical current modified the lipid dynamic behavior, trigging stearic acid crystallization in unloaded NLC and increasing drug solubilization in the lipid matrix of NLC-LPV formulation.

3.7. Drug release

Passive *in vitro* studies (without electric current) demonstrated that it was not possible to quantify LPV in the receiving compartment of diffusion cells. The high lipophilicity of LPV (log P ~x223C 4.69) prevented drug release in less than 6 h of study.

However, when cathodic or anodic iontophoresis was applied (0.5 mA/cm^2), a significantly higher release occurred, i.e. 1.33 ± 0.46% of LPV (0.71 ± 0.25 μg/cm^2) and 0.99 ± 0.11% of LPV (0.53 ± 0.06 μg/cm^2) were quantified in the receiving compartment of diffusion cells for cathodic and anodic experiments, respectively. Our research group has already observed the increased drug release by the combination of lipid-carriers and iontophoresis. We demonstrated that the combination of iontophoresis and SLN led to a significantly higher release of the drug (7.36 ± 0.74%) compared to the passive release (2.85 ± 0.74%) (Taveira et al., 2014). We discussed that the repulsion of surface charges of lipid carriers and electrodes leads to an increase in the concentration of these particles on the membrane's surface (donor compartment). The increase of drug gradient between the donor and receptor compartment, favored drug flux to the receptor compartment, increasing drug release (Taveira et al., 2014). This hypothesis could also be applied by LPV cathodic release, which was benefited by electromigration of lipids from NLC. Besides, according to our findings (electrical stability studies and EPR), it is likely that the electrical current will alter the lipid dynamics of the NLC, facilitating the partition of the drug into the aqueous medium. In this case, LPV will benefit from drug fast release and electroosmosis in anodic iontophoresis.

As demonstrated with DSC studies, the electric current contributes to the drug's solubilization in the lipid matrix. The soluble drug is ready to diffuse, unlike crystals that must solubilize and diffuse through the lipid matrix. Thus, skin permeation studies are essential to elucidate these effects on LPV skin permeation.

3.8. Drug skin permeation

Passive and iontophoretic permeation of unloaded LPV (aqueous dispersion) was performed (6 h). However, no drug was quantified in the acceptor medium, and LPV skin retention was significantly lower than observed for NLC-LPV, about 0.89 μg/cm^2 for all conditions (with and without electrical current). The lack of drug solubility in the aqueous medium may hamper its skin delivery, even if the electrical current is applied. Therefore, the molecular dispersion of the drug in the formulation is essential for iontophoretic administration (Gratieri et al., 2008, Kalia et al., 2004).

The encapsulation of the LPV in NLC, on the other hand, favored the drug skin retention and permeation to the acceptor medium of diffusion cells (Fig. 6). It is of great interest in this study that the LPV permeates the EP and reaches the diffusion cell's receptor compartment. Therefore, the combination of NLC with iontophoresis was performed to enhance drug permeation. For instance, 48 h of passive permeation of NLC-LPV resulted in a drug permeation to the receptor medium of 6.47 ± 1.82 μg/cm^2 (Fig. 6), similar to the LPV content achieved with 6 h cathodic iontophoresis ($p > 0.05$). Thus, for an effective and rapid transdermal administration, the combination of NLC and iontophoresis is the best strategy. Regarding cathodic and anodic iontophoresis, it seems that anodic iontophoresis significantly increased drug permeation ($p < 0.05$). For cathodic iontophoresis, negatively charged lipids could benefit from the electromigration. The electrical current could push the lipids, promoting close contact of NLC to the skin. Also, these nanoparticles could be directed to hair follicles, as reported in some studies, facilitating LPV permeation (Gelfuso et al., 2013; Kajimoto et al., 2011; Knorr et al., 2009; Petrilli and Lopez, 2018). These factors possibly contributed to

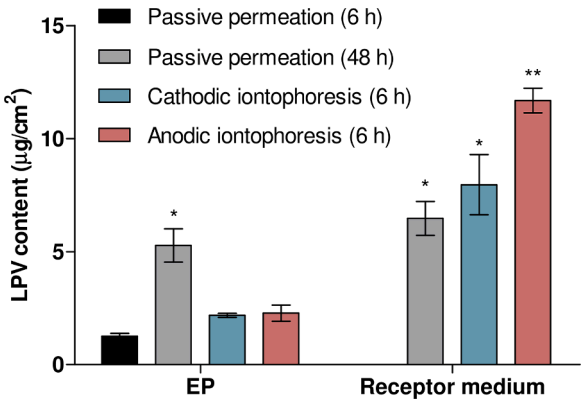

Fig. 6. Amount of LPV retained in the epidermis (EP) (μg/cm2) and quantified in the receptor medium of diffusion cells (μg/cm2), after topical administration of NLC-LPV, with and without application of cathodic and anodic iontophoresis, using a current density of 0.5 mA/cm2. Symbols indicate $p < 0.05$.

potentiate LPV permeation. Likewise, anodic iontophoresis was advantageous in increasing the permeation of the drug, significantly higher than passive and cathodic iontophoresis ($p < 0.05$). In this case, the contribution of the electroosmotic flow enhanced drug permeation to the receptor medium. Also, as already mentioned in the EPR, and release studies, the electric current probably affects the lipid matrix, which can significantly increase LPV release. In the case of anodic iontophoresis, the drug being released more quickly is ready to be transported by the electroosmotic flow, resulting in a 1.5-fold higher amount of drug in the receptor medium.

Probably, the application of iontophoresis in NLC-LPV can enable the transdermal administration of LPV *in vivo*. The amount of drug permeated *in vitro* to the receptor medium would correlate with the amount permeated *in vivo* to the dermis, where systemic absorption occurs typically. If all the drug permeated was in a blood volume of 5.5 L (approximate blood volume of an adult person), LPV concentration would be very close to the EC_{50} of LPV for different HIV (0.04 - 0.18 μg/mL, in the presence of 50% human serum) (Abbvie, 2020; Yiengst and Shock, 1962). It is important to note that the permeation results are related to a diffusion area of approximately 1.87 cm^2, suggesting that a larger diffusion area could favor obtaining concentrations of LPV effective in the control of HIV infection (Kalia et al., 2004; Saroha et al., 2011). For SARS-CoV-2 infection, the EC_{50} found was 26.63 μM (equivalent to 16.74 μg/mL). In this case, to achieve these concentrations, a larger area of application must be considered. Even so, the data suggest that the transdermal administration of LPV with a combination of NLC and iontophoresis can be a promising antiviral therapy strategy.

4. Conclusions

NLC presented nanometric size and excellent chemical and physical stability, including electrical stability. Iontophoresis favored LPV release from NLC, evidenced by the reduction of EE and faster *in vitro* release. Besides, EPR demonstrated that the faster release might be related to the decrease of lipid dynamics with the application of an electrical current. The increase of NLC rigidity occurs in the first 30 min of the experiment, and it is a long-lasting effect. DSC studies demonstrated that the electrical current trigged stearic acid crystallization in unloaded NLC and increased LPV solubilization in the lipid matrix of NLC-LPV. The permeation study showed that the combination of NLC and iontophoresis was advantageous in promoting the permeation of LPV, significantly increasing its permeation compared to the passive strategy. Also, anodic iontophoresis significantly increases drug permeation, indicating that it may be a promising strategy for this drug's transdermal administration.

CRediT authorship contribution statement

Rayssa Barbary Pedroza Moura: Conceptualization, Data curation, Writing – original draft. **Lígia Marquez Andrade:** Data curation, Writing – original draft. **Lais Alonso:** . **Antonio Alonso:** . **Ricardo Neves Marreto:** . **Stephânia Fleury Taveira:** Conceptualization, Project administration, Funding acquisition, Supervision, Writing – original draft, Writing – review & editing.

Acknowledgments

The authors would like to thank the Brazilian agencies CAPES, FAPEG, and CNPq, for financial support. LabMic/UFG for the TEM measures.

Supplementary materials

Supplementary material associated with this article can be found, in the online version, at doi:10.1016/j.ejps.2021.106048.

References

AbbVie U.S.A., 2020. Highlights of prescribing information. https://www.rxabbvie.com/pdf/kaletratabpi.pdf (accessed 28 January 2020).

Andrade, L.M., Silva, L.A.D., Krawczyk-Santos, A.P., Amorim, I.C.S.M., Da Rocha, P.B.R, Lima, E.M., Anjos, J.L.V., Alonso, A, Ricardo Neves Marreto, R.N., Taveira, S.F., 2017. Improved tacrolimus skin permeation by co-encapsulation with clobetasol in lipid nanoparticles: study of drug effects in lipid matrix by electron paramagnetic resonance. Eur. J. Pharm. Biopharm. 119, 142–149. https://doi.org/10.1016/j.ejpb.2017.06.014.

Ansari, H., Singh, P., 2018. Formulation and in-vivo evaluation of novel topical gel for lopinavir for targeting HIV. Curr. Hiv Res. 16 (4), 270–279. https://doi.org/10.2174/1570162X16666180924101650.

Behbahani, E.S., Ghaedi, M., Abbaspour, M., Rostamizadeh, K., 2017. Optimization and characterization of ultrasound assisted preparation of curcumin-loaded solid lipid nanoparticles: application of central composite design, thermal analysis and X-ray diffraction techniques. Ultrason. Sonochem. 38, 271–280. https://doi.org/10.1016/j.ultsonch.2017.03.013.

Charoenputtakun, P., Li, S.K., Ngawhirunpat, T., 2015. Iontophoretic delivery of lipophilic and hydrophilic drugs from lipid nanoparticles across human skin. Int. J. Pharm. 495 (1), 318–328. https://doi.org/10.1016/j.ijpharm.2015.08.094.

Chopra, P., Hao, J., Li, S.K., 2013. Influence of drug lipophilicity on drug release from sclera after iontophoretic delivery of mixed micellar carrier system to human sclera. J. Pharm. Sci. 102 (2), 480–488. https://doi.org/10.1002/jps.23370.

Chopra, P., Hao, J., Li, S.K., 2012. Sustained release micellar carrier systems for iontophoretic transport of dexamethasone across human sclera. J. Control Release 160 (1), 96–104. https://doi.org/10.1016/j.jconrel.2012.01.032.

Czajkowska-Kośnik, A., Szekalska, M., Winnicka, K., 2019. Nanostructured lipid carriers: a potential use for skin drug delivery systems. Pharmacol. Rep. 71 (1), 156–166. https://doi.org/10.1016/j.pharep.2018.10.008.

Da Rocha, P.B.R., Souza, B.S., Andrade, L.M., Dos Anjos, J.L.V., Mendanha, S.A., Alonso, A., Marreto, R.N., Taveira, S.F., 2019. Enhanced asiaticoside skin permeation by Centella asiatica-loaded lipid nanoparticles: effects of extract type and study of stratum corneum lipid dynamics. J. Drug Deliv. Sci. Technol. 50, 305–312. https://doi.org/10.1016/j.jddst.2019.01.016.

De Queirós, W.P., Neto, D.S., Alonso, A., 2005. Dynamics and partitioning of spin-labeled stearates into the lipid domain of stratum corneum. J. Control. Release 106 (3), 374–385. https://doi.org/10.1016/j.jconrel.2005.05.009.

Diaz, R.S., 2016. Potência e barreira genética dos medicamentos e esquemas antirretrovirais. Braz. J. Infec. Dis. 2 (3), 70–81.

Fang, C.L., Al-Suwayeh, S.A., Fang, .J..-Y., 2013. Nanostructured lipid carriers (NLCs) for drug delivery and targeting. Recent Pat. Nanotechnol. 7 (1), 41–55. https://doi.org/10.2174/187221051130701.

Fang, J.Y., Sung, K.C., Lin, H.H., Fang, C.L., 1999. Transdermal iontophoretic delivery of enoxacin from various liposome-encapsulated formulations. J. Control Release 60 (1), 1–10. https://doi.org/10.1016/s0168-3659(99)00055-3.

Garcês, A., Amaral, M.H., Sousa Lobo, J.M., Silva, A.C., 2018. Formulations based on solid lipid nanoparticles (SLN) and nanostructured lipid carriers (NLC) for cutaneous use: a review. Eur. J. Pharm. Sci. 112, 159–167. https://doi.org/10.1016/j.ejps.2017.11.023.

Garg, B., Beg, S., Kumar, R., Katare, O.P., Singh, B., 2019. Nanostructured lipid carriers of lopinavir for effective management of HIV-associated neurocognitive disorder. J. Drug Deliv. Sci. Technol. 53 (101220) https://doi.org/10.1016/j.jddst.2019.101220.

Gelfuso, G.M., Gratieri, T., Delgado-Charro, M.B., Guy, R.H., Lopez, R.F.V., 2013. Iontophoresis-targeted, follicular delivery of minoxidil sulfate for the treatment of alopecia. J. Pharm. Sci. 102 (5), 1488–1494. https://doi.org/10.1002/jps.23485.

Gordillo-Galeano, A., Mora-Huerta, C.E., 2021. Hydrodynamic diameter and zeta potential of nanostructured lipid carriers: emphasizing some parameter of correct measurements. Colloids Surf. A. Physicochem. Eng. Asp. 620, 126610 https://doi.org/10.1016/j.colsurfa.2021.126610.

Ghosn, J., Taiwo, B., Seedat, S., Autran, B., Katlama, C., 2018. HIV. Lancet. 392 (10148), 685–697. https://doi.org/10.1016/S0140-6736(18)31311-4.

Gordillo-Galeano, A., Mora-Huertas, C.E., 2018. Solid lipid nanoparticles and nanostructured lipid carriers: a review emphasizing on particle structure and drug release. Eur. J. Pharm. Biopharm. 133, 285–308. https://doi.org/10.1016/j.ejpb.2018.10.017.

Gratieri, T., Gelfuso, G.M., Lopez, R.F.V., 2008. Princípios básicos e aplicação da iontoforese na penetração cutânea de fármacos. Química Nova 31 (6), 1490–1498. https://doi.org/10.1590/S0100-40422008000600040.

Huber, L.A., Pereira, T.A., Ramos, D.N., Rezende, L.C., Emery, F.S., Sobral, L.M., Leopoldino, A.M., Lopez, R.F., 2015. Topical skin cancer therapy using doxorubicin-loaded cationic lipid nanoparticles and lontophoresis. J. Biomed. Nanotechnol. 11 (11), 1975–1988. https://doi.org/10.1166/jbn.2015.2139.

Iannazzo, D., Pistone, A., Romeo, R., Giofrè, S.V., 2015. Nanotechnology approaches for antiretroviral drugs delivery. J. Aids HIV Infect. 1 (2) https://doi.org/10.15744/2454-499X.1.201.

Jores, K., Mehnert, W., Mäder, K., 2003. Physicochemical investigations on solid lipid nanoparticles and on oil-loaded solid lipid nanoparticles: a nuclear magnetic resonance and electron spin resonance study. Pharm. Res. 20 (8), 1274–1283. https://doi.org/10.1023/A:1025065418309.

Kajimoto, K., Kajimoto, K., Yamamoto, M., Watanabe, M., Kigasawa, K., Kanamura, K., Harashima, H., Kogure, K., 2011. Non-invasive and persistent transfollicular drug delivery system using a combination of liposomes and iontophoresis. Int. J. Pharm. 403 (1–2), 57–65. https://doi.org/10.1016/j.ijpharm.2010.10.021.

Kalia, Y.N., Naika, A., Garrisonc, J., Guy, R.H., 2004. Iontophoretic drug delivery. Adv. Drug Deliv. Rev. 56 (5), 619–658. https://doi.org/10.1016/j.addr.2003.10.026.

Kim, K.T., Lee, J., Kim, M.H., Park, J.H., Lee, J.Y., Song, J.H., Jung, M., Jang, M.H., Cho, H.J., Yoon, I.S., Kim, D.D., 2017. Novel reverse electrodialysis-driven iontophoretic system for topical and transdermal delivery of poorly permeable therapeutic agents. Drug Deliv. 24 (1), 1204–1215. https://doi.org/10.1080/10717544.2017.1367975.

Knorr, F., Lademann, J., Patzelt, A., Sterry, W., Blume-Peytavi, U., Vogt, A., 2009. Follicular transport route – Research progress and future perspectives. Eur. J. Pharm. Biopharm. 71 (2), 173–180. https://doi.org/10.1016/j.ejpb.2008.11.001.

Krishnan, G., Roberts, M.S., Grice, J., Anissimov, Y.G., Moghimi, H.R., Benson, H.A.E., 2014. Iontophoretic skin permeation of peptides: an investigation into the influence of molecular properties, iontophoretic conditions and formulation parameters. Drug Deliv. Transl. Res. 4, 222–232. https://doi.org/10.1007/s13346-013-0181-8.

Liu, F., Xu, A., Zhang, Y., Xuan, W., Yan, T., Pan, K., Yu, W., Zhang, J., 2020. Patients of COVID-19 may benefit from sustained lopinavir-combined regimen and the increase of eosinophil may predict the outcome of COVID-19 progression. Int. J. Infect. Dis. 95, 183–191. https://doi.org/10.1016/j.ijid.2020.03.013.

Maniyar, M.G., Kokare, C.R., 2019. Formulation and evaluation of spray dried liposomes of lopinavir for topical application. J. Pharm. Investig. 49, 259–270. https://doi.org/10.1007/s40005-018-0403-7.

Maretti, E., Leo, E., Rustichelli, C., Truzzi, E., Siligardi, C., Innuccelli, V., 2021. *In vivo* β-carotene skin permeation modulated by nanostructured lipid carriers. Int. J. Pharm. 597, 120322 https://doi.org/10.1016/j.ijpharm.2021.120322, 2021.

Mitri, K., Shegokar, R., Gohla, S., Anselmi, C., Müller, R.H., 2011. Lipid nanocarriers for dermal delivery of lutein: preparation, characterization, stability and performance. Int. J. Pharm. 414 (1–2), 267–275. https://doi.org/10.1016/j.ijpharm.2011.05.008.

Montenegro, L., Lai, F., Offerta, A., Sarpietro, M.G., Micicchè, L., Maccioni, A.M., Valenti, D., Fadda, A.M., 2016. From nanoemulsions to nanostructured lipid carriers: a relevant development in dermal delivery of drugs and cosmetics. J. Drug Deliv. Sci. Technol. 32, 100–112. https://doi.org/10.1016/j.jddst.2015.10.003.

Negi, J.S., Chattopadhyay, P., Sharma, A.K., Ram, V., 2013. Development of solid lipid nanoparticles (SLNs) of lopinavir using hot self nano-emulsification (SNE) technique. Eur. J. Pharm Sci. 48 (1–2), 231–239. https://doi.org/10.1016/j.ejps.2012.10.022.

Patel, D., Kumar, P., Thakkar, H.P., 2015. Lopinavir metered-dose transdermal spray through microporated skin: permeation enhancement to achieve therapeutic needs. J. Drug Deliv. Sci. Technol. 29, 173–180. https://doi.org/10.1016/j.jddst.2015.07.004.

Patel, G., Shelat, P., Lalwani, A., 2016. Statistical modeling, optimization and characterization of solid self-nanoemulsifying drug delivery system of lopinavir using design of experiment. Drug Deliv. 23 (8), 3027–3042. https://doi.org/10.3109/10717544.2016.1141260.

Patel, K.K., Gade, S., Anjum, Md.M., Sanjay Kumar Singh, S.K., Maiti, P., Agrawal, A.K., Sanjay Singh, S., 2019. Effect of penetration enhancers and amorphization on transdermal permeation flux of raloxifene-encapsulated solid lipid nanoparticles: an *ex vivo* study on human skin. Appl. Nanosci. 9, 1383–1394. https://doi.org/10.1007/s13204-019-01004-6.

Patel, K.K., Kumar, P., Thakkar, H.P., 2012. Formulation of niosomal gel for enhanced transdermal lopinavir delivery and its comparative evaluation with ethosoma gel. AAPS PharmSciTec 13 (4), 1502–1510. https://doi.org/10.1208/s12249-012-9871-7.

Petrilli, R., Lopez, R.F.V., 2018. Physical methods for topical skin drug delivery: concepts and applications. Braz. J. Pharm. Sci. 54. https://doi.org/10.1590/s2175-97902018000001008 e01008.

Pham, K., Li, D., Guo, S., Penzak, S., Dong, X., 2016. Development and *in vivo* evaluation of child-friendly lopinavir/ritonavir pediatric granules utilizing novel in situ self-assembly nanoparticles. J. Control. Release 226, 88–97. https://doi.org/10.1016/j.jconrel.2016.02.001.

Puri, A., Sivaraman, A., Zhang, W., Meredith R Clark, M.R., Banga, A.K., 2017. Expanding the domain of drug delivery for HIV prevention: exploration of the

transdermal route. Critic. Rev. Ther. Drug Carrier Syst. 34 (6), 551–587. https://doi.org/10.1615/CritRevTherDrugCarrierSyst.2017020147.

Ravi, P.R., Vats, R., Dalal, V., Gadekar, N., Aditya, N., 2015. Design, optimization and evaluation of poly-e-caprolactone (PCL) based polymeric nanoparticles for oral delivery of lopinavir. Drug Dev. Ind. Pharm. 41 (1), 131–140. https://doi.org/10.3109/03639045.2013.850710.

Santos, G.A., Angelo, T., Andrade, L.M., Silva, S.M.M., Magalhães, P.O., Cunha-Filho, M., Gelfuso, G.M., Taveira, S.F., Gratieri, T., 2018. The role of formulation and follicular pathway in voriconazole cutaneous delivery from liposomes and nanostructured lipid carriers. Colloids Surf. B Biointerfaces 170, 341–346. https://doi.org/10.1016/j.colsurfb.2018.06.037.

Saroha, K., Yadav, B., Sharma, B., 2011. Transdermal patch: a discrete dosage form. Int. J. Curr. Pharm. Res. 3 (3).

Sarvaiya, J.I., Kapse, G., K, Tank, C, J., 2013. Iontophoresis of micellar composition of lovastatin: study of affecting factors and in-vitro permeation. J. Pharm. Res. 7 (4), 327–330. https://doi.org/10.1016/j.jopr.2013.04.032.

Shah, C.V., Shah, V., Upadhyay, U., 2011. Solid lipid nanoparticles: a review. Curr. Pharma Res. 1 (4), 351–368.

Sato, Katsuya, 1987. Physical and Molecular Properties of Lipid Polymorphs - A Review. Food Structure 6 (2), 151–159.

Shah, R.M., Malherbe, F., Eldridge, D., Palombo, E., Harding, I.H., 2014. Physicochemical characterization of solid lipid nanoparticles (SLNs) prepared by a novel microemulsion technique. J. Colloid Interface Sci. 428, 286–294. https://doi.org/10.1016/j.jcis.2014.04.057.

Silva, L.A.D., Andrade, L.M., De Sá, F.A.P., Marreto, R.N., Lima, E.M., Gratieri, T., Taveira, S.F., 2016. Clobetasol-loaded nanostructured lipid carriers for epidermal targeting. J. Pharm. Pharmacol. 68 (6), 742–750. https://doi.org/10.1111/jphp.12543.

Silva, L.A.D., Taveira, S.F., Lima, E.M., Marreto, R.N., 2012. *In vitro* skin penetration of clobetasol from lipid nanoparticles: drug extraction and quantitation in different skin layers. Braz. J. Pharm. Sci. 48 (4) https://doi.org/10.1590/S1984-82502012000400025.

Souza, L.G., Silva, E.J., Martins, A.L.L., Mota, M.F., Braga, R.C., Lima, E.M., Valadares, M.C., Taveira, S.F., Marreto, R.N., 2011. Development of topotecan loaded lipid nanoparticles for chemical stabilization and prolonged release. Eur. J. Pharm. Biopharm. 79 (1), 189–196. https://doi.org/10.1016/j.ejpb.2011.02.012.

Stella, B., Peira, E., Dianzani, C., Gallarate, M., Battaglia, L., Gigliotti, C.L., Boggio, E., Dianzani, U., Dosio, F., 2018. Development and characterization of solid lipid nanoparticles loaded with a highly active doxorubicin derivative. Nanomaterials 8 (2), 110. https://doi.org/10.3390/nano8020110.

Taveira, S.F., Araújo, L.M.P.C., De Santana, D.C.A.S., Nomizo, A., De Freitas, L.A.P., Lopez, R.F.V., 2012. Development of cationic solid lipid nanoparticles with factorial design-based studies for topical administration of doxorubicin. J. Biomed. Nanotechnol. 8, 219–228. https://doi.org/10.1166/jbn.2012.1383.

Taveira, S.F., De Santana, D.C.A.S., Araújo, L.M.P.C., Marquele-Oliveira, F., Nomizo, A., Lopez, R.F.V., 2014. Effect of iontophoresis on topical delivery of doxorubicin-loaded solid lipid nanoparticles. J. Biomed. Nanotechnol. 10, 1382–1390. https://doi.org/10.1166/jbn.2014.1834.

Teixeira, A.C.T., Garcia, A.R., Ilharco, L.M., Silva, A.M.P.S.G., Fernandes, A.C., 2010. Phase behavior of oleanolic acid, pure and mixed with stearic acid: interactions and crystallinity. Chem. Phys. Lipids (7), 163. https://doi.org/10.1016/j.chemphyslip.2010.06.001.

Teixeira, F.V., Alves, G.L., Ferreira, M.H., Taveira, S.F., Cunha-Filho, M.S.S., Marreto, R. N, 2018. Preformulation studies to guide the development of raloxifene lipid-based delivery systems. J. Therm. Anal. Calorim. 132 (1), 365–371. https://doi.org/10.1007/s10973-018-6964-x.

Tosta, F.V., Andrade, L.M., Mendes, L.P., Anjos, J.L.V., Alonso, A., Marreto, R.N., Lima, E.M., Taveira, S.F., 2014. Paclitaxel-loaded lipid nanoparticles for topical application: the influence of oil content on lipid dynamic behavior, stability, and drug skin penetration. J. Nanopart. Res. 16 (2782) https://doi.org/10.1007/s11051-014-2782-7.

Wang, C., Zhu, J., Zhang, D., Yang, Y., Zheng, L., Qu, Y., Yang, X., Cui, X., 2018. Ionic liquid – microemulsions assisting in the transdermal delivery of Dencichine: preparation, in-vitro and in-vivo evaluations, and investigation of the permeation mechanism. Int. J. Pharm. 535 (1–2), 120–131. https://doi.org/10.1016/j.ijpharm.2017.10.024.

Yiengst, M.J., Shock, N.W., 1962. Blood and plasma volume in adult males. J. Appl. Physiol. 17, 195–198. https://doi.org/10.1152/jappl.1962.17.2.195.

Zhong, Q., Zhang, L., 2019. Nanoparticles fabricated from bulk solid lipids: preparation, properties, and potential food applications. Adv. Colloid Interface Sci. 273 (102033) https://doi.org/10.1016/j.cis.2019.102033.

Zimmermann, E., Müller, R.H., 2001. Electrolyte – and pH – stabilities of aqueous solid lipid nanoparticle (SLN ™) dispersions in artificial gastrointestinal media. Eur. J. Pharm. Biopharm. 52 (2), 203–210. https://doi.org/10.1016/S0939-6411(01)00167-9.